REPORT

TOPOLOGICAL OPTICS

Observation of Floquet solitons in a topological bandgap

Sebabrata Mukherjee* and Mikael C. Rechtsman*

Topological protection is a universal phenomenon that applies to electronic, photonic, ultracold atomic, mechanical, and other systems. The vast majority of research in these systems has explored the linear domain, where interparticle interactions are negligible. We experimentally observed solitons—waves that propagate without changing shape as a result of nonlinearity—in a photonic Floquet topological insulator. These solitons exhibited distinct behavior in that they executed cyclotron-like orbits associated with the underlying topology. Specifically, we used a waveguide array with periodic variations along the waveguide axis, giving rise to nonzero winding number, and the nonlinearity arose from the optical Kerr effect. This result applies to a range of bosonic systems because it is described by the focusing nonlinear Schrödinger equation (equivalently, the attractive Gross-Pitaevskii equation).

The discovery of the integer quantum Hall effect (*1*) and its topological interpretation (*2*) initiated extensive research into exotic topological materials in a wide variety of platforms (*3*–*14*). The prediction of quantum Hall-like states for light (*3*) has led to wide interest (*15*, *16*) in the interplay between topological protection and photonic properties, especially effects that are not realized for electrons in solids. After its first observation in a gyromagnetic photonic crystal at microwave frequencies (*4*), topological edge states were demonstrated at optical frequencies in waveguide lattices (*5*) and in ring resonators (*6*). The investigation into topological states in electromagnetic systems has been largely limited to the linear domain, where photons propagate independently, governed by Maxwell's equations. These topological states are described as a system of noninteracting particles with topologically nontrivial bands, characterized by integer-valued invariants such as Chern numbers.

Among the most fundamental effects in nonlinear optics is the Kerr effect: a variation of the refractive index proportional to the local intensity of light. This intensity-dependent refractive index is a manifestation of the nonlinear dielectric polarization induced by optical fields. Thus, at high intensity, photons can effectively interact, mediated by the ambient medium. Indeed, the nonlinear Schrödinger equation describing the propagation of light through a nonlinear medium is equivalent to the Gross-Pitaevskii equation, which describes bosonic interactions in a Bose-Einstein condensate in the mean-field limit. Hence, photonic lattices are a natural platform for studying the interplay of topology and interparticle interactions.

Here, we observed optical spatial solitons (*17*–*22*) in an anomalous Floquet topological insulator (*23*–*25*), realized using a periodically modulated waveguide lattice. For such a topological phase, the Floquet driving gives rise to a nonzero winding number, implying the presence of topological edge modes (*23*); however, the standard topological invariants (e.g., Chern numbers) are zero (hence the name "anomalous"). A family of solitons spectrally resides in the topological bandgap, and during propagation, the solitons execute cyclotron-like rotations inherited from the linear host lattice (we henceforth refer to a soliton in a topological bandgap as a "topological soliton"). Consistent with previous theoretical predictions of topological solitons, these solitons show behavior that arises from the topological nature of the system (*26*–*29*). Indeed, the cyclotron-like motion defines the topological character of the solitons: In the quantum Hall effect, the cyclotron motion gives rise to the "skipping orbits" that describe protected edge states (*30*). In that sense, these solitons are of a different nature from that of previously observed bandgap solitons.

In the presence of the optical Kerr effect, light propagation through a photonic lattice with nearest-neighbor evanescent coupling is described by the discrete nonlinear Schrödinger equation, under the paraxial approximation:

$$i\frac{\partial}{\partial z}\phi_s(z) = \sum_{\langle s' \rangle} H_{ss'}\phi_{s'} - |\phi_s|^2\phi_s \qquad (1)$$

where the propagation distance (z) plays the role of time ($z \leftrightarrow t$), and $H_{ss'}$ is the linear tight-binding Hamiltonian (the summation is over neighboring sites only). We define $|\phi_s|^2 = g|\psi_s|^2$ where $|\psi_s|^2$ is the optical power at the sth waveguide and g is determined by the nonlinear refractive index coefficient, the effective area of the waveguide modes, and the wavelength. At sufficiently low optical power, the nonlinear term of Eq. 1 is negligible. Here, we have used the self-focusing nonlinearity (corresponding to attractive interactions in the Gross-Pitaevskii equation), which was experimentally validated for the nonlinear medium used here (*31*). In the absence of optical losses, the total energy and the renormalized

Department of Physics, The Pennsylvania State University, University Park, PA 16802, USA.
*Corresponding author. Email: mukherjeesebabrata@gmail.com (S.M.); mcrworld@psu.edu (M.C.R.)

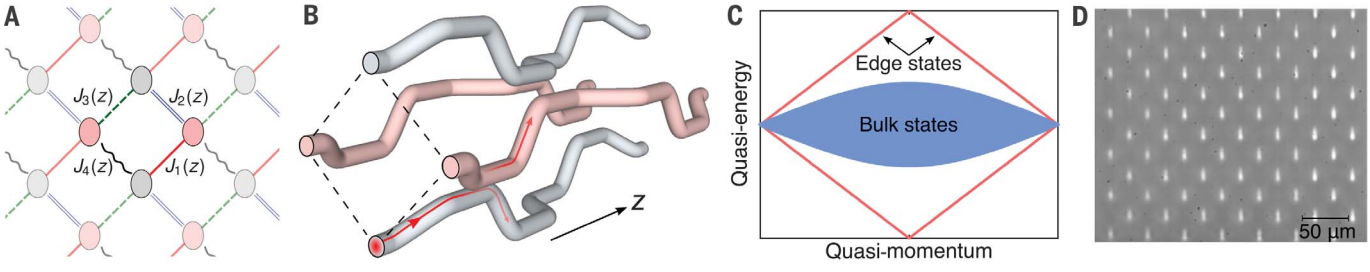

Fig. 1. Photonic implementation of an anomalous Floquet topological insulator. (**A**) A periodically driven square lattice where the four equal couplings $J_m(z)$ [m = 1, ..., 4] are switched on and off in a cyclic (spatially and z periodic) manner. (**B**) Schematic showing how this driving protocol is implemented using three-dimensional waveguide arrays. Only four sites are shown here for one complete driving period, z_0. (**C**) Quasi-energy spectrum in the linear regime (for the experimentally realized parameters) showing two ungapped bulk bands with zero net Chern number and chiral edge modes. (**D**) Micrograph of the facet of a driven photonic square lattice fabricated by femtosecond laser writing.

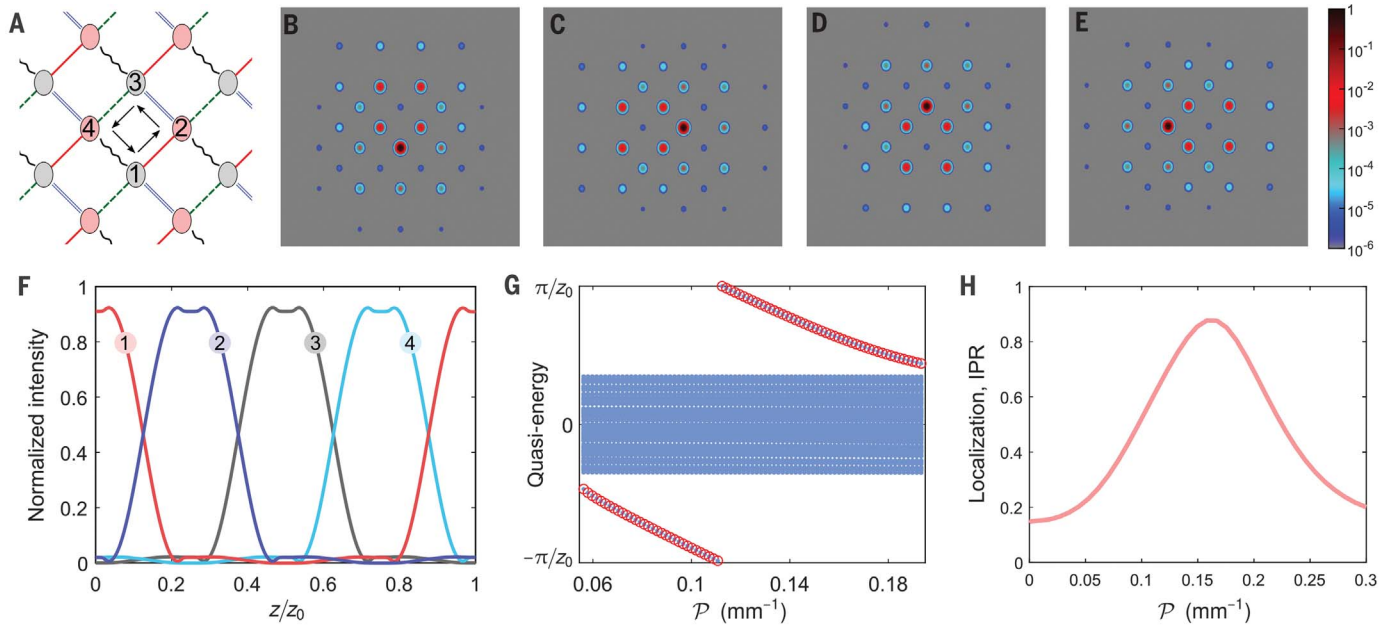

Fig. 2. Topological bandgap soliton performing cyclotron-like motion. (**A**) Schematic showing the four sites (1 to 4) where the maximum optical power of a topological soliton is contained during propagation. (**B** to **E**) Normalized intensity profile of a soliton (at $\mathcal{P}$ = 0.088 mm^{-1}) rotating counterclockwise and cycling back to itself after each complete period of driving; the color map is in log scale. Here, the soliton profile is shown for each quarter of a complete period—that is, $z = \{0, 1, 2, 3\}z_0/4$. (**F**) Variation of normalized intensity at the four sites [1 to 4 in (A)] showing the dynamics in a complete period. (**G**) Quasi-energy as a function of renormalized power, showing the family of bulk solitons (red circles) on both sides of the linear modes. (**H**) A signature of topological solitons: When light is coupled to a single bulk waveguide, the output intensity pattern at $z = 2z_0$ exhibits a distinct feature: a peak in the inverse participation ratio (IPR), which is detected in experiments (see Fig. 3).

power ($\mathcal{P} \equiv \sum_s |\phi_s|^2$) are conserved. Nonlinearity in the off-diagonal coupling term is negligible.

Consider a periodically modulated photonic square lattice (*24*, *25*, *32*) with nearest-neighbor couplings $J_m(z)$ [m = 1, ..., 4] that are engineered in a cyclic (spatially and z periodic) manner such that every waveguide is coupled to only one of its nearest neighbors at a given propagation distance z (Fig. 1, A and B). The driving period z_0 is split into four equal steps, and over each quarter of the driving period, only one of the four couplings is switched on, with a fixed $\Lambda = \int \mathrm{d}z J_m(z)$ (the integral is taken over one coupling operation). In the linear regime, the quasi-energy spectrum can be obtained by diagonalizing the Floquet evolution operator over one period, defined as

$$\hat{U}(z_0) = \mathcal{T}\exp\left[-i\int_0^{z_0} \hat{H}(\tilde{z})\mathrm{d}\tilde{z}\right] \qquad (2)$$

where $\mathcal{T}$ indicates the "time" ordering and $\hat{H}(z) = \hat{H}(z + z_0)$ is the periodic linear Hamiltonian. This driven lattice supports two ungapped bulk bands (henceforth referred to as the bulk band), and the bandwidth is determined by Λ: For $\Lambda = \pi/2$, the bulk band becomes perfectly flat, and the bandgap closes at $\Lambda = \{\pi/4, 3\pi/4\}$. To experimentally realize a weakly dispersive bulk band with an appreciable bandgap, we set $\Lambda = 1.85 \pm 0.05$. The ratio of the bulk bandwidth to the maximal coupling strength max[$J(z)$] is estimated to be ~0.25, which quantifies the flatness of the band (whereas the bandwidth of a standard static square lattice is eight times the coupling strength). Figure 1C shows a spectrum calculated for a strip geometry aligned along the vertical direction and periodic along the horizontal direction. As a result of the periodicity of quasi-energy, the edge modes can cross the bandgap, connecting the top and bottom of the band structure. A single chiral edge mode exists above and below the bulk band (propagating in the same direction on a given edge), which implies that the Chern number of the bulk band is zero. For such anomalous Floquet topological insulators (*23*, *33*), the topology can be captured using a different topological invariant, the winding number (*31*). This scenario can only arise in the presence of suitable time-periodic driving; anomalous Floquet topological insulators have no analog in static systems. There is only one bandgap in the system (Fig. 1C), and it is topological.

Using a self-consistency method modified for Floquet systems (*26*), we sought localized nonlinear solutions (solitons) in this modulated photonic square lattice (*31*). The result is solitons in the Floquet sense: Because of the z-periodic driving, the solitons reproduce themselves after each complete period (up to a phase factor), although micromotion within the Floquet cycle is allowed for. The solitons continuously rotate, performing cyclotron-like motion (movie S1). Figure 2, B to E, shows the normalized intensity profile (i.e., $|\phi_s|^2/\mathcal{P}$) of a soliton at each quarter-period (i.e., $z = \{0, 1, 2, 3\}z_0/4$). Figure 2F shows the variation of normalized intensity at the four sites (1 to 4 in Fig. 2A) where the maximum optical power of the soliton is supported during propagation.

The quasi-energy of a soliton is determined by the overall phase acquired after the propagation of one driving period (ε = phase/z_0). The quasi-energy spectrum, plotted as a function of the renormalized power (Fig. 2G), shows a family of bandgap solitons (red circles) bifurcating from the linear band (blue). The size (i.e., the spatial extent) of the solitons first decreases as a function of power, showing maximal localization near the mid-gap quasi-energy π/z_0. When the power is further increased, these Floquet solitons become delocalized as they approach the band from the other side (*31*)—a behavior unlike that of standard lattice solitons. In other words, for a given dispersion of the linear band, the spatial extent of these solitons is determined by their quasi-energy; solitons closer in energy to the linear band have a larger spatial extent (movie S2). Because the solitons are strongly

peaked on a single site, it is possible to probe them in experiments by means of single-site excitation (i.e., by coupling light into a single waveguide). A signature of these bandgap solitons can be experimentally detected by measuring the degree of localization of the output intensity patterns as a function of renormalized power. We plot the inverse participation ratio

$$\mathrm{IPR} \equiv \frac{\sum |\phi_s|^4}{\left(\sum |\phi_s|^2\right)^2} \qquad (3)$$

(a measure of localization), after two driving periods, in Fig. 2H. Here, we observed a clear peak in the IPR, corresponding to the existence and strong localization of these gap solitons. We note that the peak occurs at an input power higher than the power of the soliton at its most localized; this is because we do not input the exact soliton wave function but rather a single site, meaning that some power is lost to background radiation in the lattice. The trend in IPR (i.e., delocalization to localization to delocalization) is qualitatively different from the trend in a topologically trivial static lattice, where IPR continuously increases and then saturates at very high nonlinearity (*31*).

To demonstrate how topological solitons are distinct from trivial ones, we examined the area encircled by the center of mass of the soliton, which acts as a quantitative measure of whether the orbit can be considered "cyclotron-like." We found that this area is finite for any soliton in a topologically nontrivial gap and is zero for any soliton in a topologically trivial gap; these findings correspond directly to the cyclotron-like nature of the soliton micromotion in the topological case. As a stark example of this fact, we give an example of two different families of solitons that reside in the same lattice: one in a topological gap with nonzero encircled area, and one in a trivial gap with zero encircled area (*31*).

To experimentally probe the solitons described above, we coupled intense laser pulses into femtosecond laser–fabricated waveguide arrays [see (*31*) for fabrication details]. In this situation, ϕ_s is a function of both propagation distance and time t: $\phi_s = \phi_s(z, t)$. Because of the temporal shape of light pulses, self-phase modulation and chromatic dispersion are relevant. Laser pulses were temporally stretched (to $t_p \approx 2$ ps) and down-chirped such that these effects could be ignored (*31*). Additionally, we found that the insertion loss is independent of nonlinearity, implying negligible nonlinear loss due to multiphoton absorption. To validate these claims, we performed experiments with a topologically trivial static square lattice consisting of straight coupled waveguides. We observed that the output intensity pattern became increasingly localized as a function of input power, and finally, all the optical power was trapped largely in the single site where the light was launched at the input (*31*) (movie S3), as expected. This baseline experiment clearly demonstrates the formation of highly localized solitons in a topologically trivial bandgap (*22*, *34*).

For the topological case, a 76-mm-long periodically modulated square lattice of 84 sites was fabricated with the previously mentioned driving parameters; a micrograph of this lattice (cross section) is shown in Fig. 1D. Initially, the waveguides were separated by 26.5 μm such that the evanescent couplings were negligibly small. To couple any two desired waveguides, we first reduced the inter-waveguide separation by synchronously bending the waveguide paths, then kept the two waveguides parallel with 14.5-μm fixed center-to-center spacing, and finally separated them (Fig. 1B).

Nonlinear characterization of the photonic lattice is summarized in Fig. 3. For all measurements, we launched light pulses into a bulk waveguide away from the edges; during linear diffraction, the light did not reach the sides of the array, and thus any edge effects could be neglected. As detailed in (*31*), the renormalized power $\mathcal{P}$ at the input of the lattice was found to be 0.076 mm^{-1} per unit average input power in mW (note that $\mathcal{P}$ has the same dimension as the evanescent coupling strength, for clarity). In the first set of experiments, we measured output intensity distributions at $z = 2z_0$ as a function of average input power (movie S4). The variation of IPR with input power is shown in Fig. 3A. At low optical power (i.e., in the linear regime), this single-site excitation overlapped with the weakly dispersive bulk modes, and light diffracted away from the site into which it was injected (Fig. 3B). As input power was increased, output intensity patterns became increasingly localized, exhibiting a peak in the IPR near average power $P = 3.4$ mW (Fig. 3C). Most of the optical power in Fig. 3C was contained at the site where the light was initially launched (indicated by the red arrow). When the power was further increased, the output showed a marked delocalization (Fig. 3D), as would be expected from the numerical result presented in Fig. 2H.

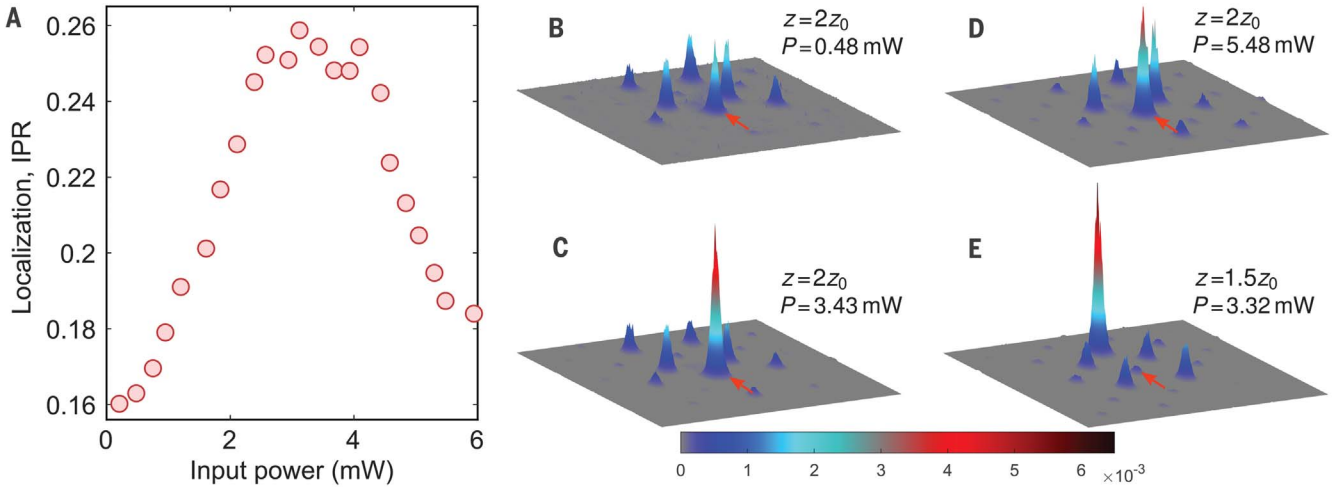

Fig. 3. Experimental observation of topological bandgap solitons. (**A**) IPR as a function of average input power measured at $z = 2z_0$. The presence of the peak corresponds to the existence of the topological bandgap solitons. For these measurements, $\mathcal{P}$ at the input of the lattice was found to be 0.076 mm^{-1} per unit average input power in mW. (**B** to **D**) Corresponding output intensity distributions for three different input powers. The red arrow in each image indicates the site where the light was launched at the input. (**E**) Most localized output intensity distribution measured at $z = 1.5z_0$. Note that the brightest site in this case is located directly across a diagonal from the site where the light was launched, corresponding to the cyclotron-like motion of the solitons. The field of view is smaller than the actual lattice size. Each experimentally observed intensity pattern is normalized.

In a second set of experiments, we used a similar photonic lattice with maximum propagation distance $z_{max} = 1.5z_0$ instead of $2z_0$ (movie S5). The IPR in this case exhibited a similar behavior (i.e., delocalization to localization to delocalization) to Fig. 3A. The most localized output intensity pattern was observed near $P = 3.3$ mW (see Fig. 3E). In contrast to Fig. 3C, the brightest site in Fig. 3E was not located where the light was initially launched but was in another waveguide that was directly across a diagonal from the injected site; this constitutes direct evidence of the cyclotron-like motion of the solitons. Comparing Fig. 2H and Fig. 3A, the peak of IPR is experimentally observed at a higher power ($\mathcal{P} = 0.26$ mm^{-1}) and the contrast of the peak is lower than what is expected from theory, as a result of linear loss. Additionally, the front and rear tails (in time) of the pulses behaved linearly, producing a small background and causing a lower contrast in IPR. That said, the observed peak in IPR is a clear signature of the topological bandgap solitons.

Our ability to control the "flatness" of the bulk band by tailoring the coupling parameter Λ is key to the observation of these solitons. In solid-state systems, flat bands play an important role in enhancing the relative strength of interactions [a recent example is twisted bilayer graphene (*35*)]. This is also true in our case but in a different way: The width of the linear band sets the power threshold of solitons in two dimensions. In the extreme case of a perfectly flat band, all linear Bloch states are degenerate, and thus localized eigenstates can be constructed as a superposition of these states, implying that stationary states exist even in the linear domain. Thus, in this limit, solitons have zero power threshold. Operating near the flat band with an appreciable bandgap allows us to probe the solitons at an experimentally accessible power value.

The observation of topological solitons opens a new avenue in the investigation of topological nonlinear optics, complementing other platforms such as Rydberg polaritons (*36*) and nonlinear circuits (*37*). Furthermore, nonlinearity can act as a means to modify (*38*, *39*) and probe (*40*, *41*) topological photonic structures. There are many open questions; for example, the degree of robustness and the stability properties of chiral edge states in the presence of nonlinearity are unknown. It will also be of central importance to define new invariants that characterize the observable behavior of nonlinear topological systems. The interplay of nonlinearity and disorder in topological systems will be necessary if nonlinear topological devices are to be of technological use. We expect that these issues, among others, will dictate how topological states can be incorporated in useful devices based on wave mechanics, whether in the photonic, acoustic/phononic, optomechanical, atomic, polaritonic, or other domains.

REFERENCES AND NOTES

1. K. von Klitzing, G. Dorda, M. Pepper, *Phys. Rev. Lett.* **45**, 494–497 (1980).
2. D. J. Thouless, M. Kohmoto, M. P. Nightingale, M. den Nijs, *Phys. Rev. Lett.* **49**, 405–408 (1982).
3. S. Raghu, F. D. M. Haldane, *Phys. Rev. A* **78**, 033834 (2008).
4. Z. Wang, Y. Chong, J. D. Joannopoulos, M. Soljačić, *Nature* **461**, 772–775 (2009).
5. M. C. Rechtsman *et al.*, *Nature* **496**, 196–200 (2013).
6. M. Hafezi, S. Mittal, J. Fan, A. Migdall, J. M. Taylor, *Nat. Photonics* **7**, 1001–1005 (2013).
7. M. Atala *et al.*, *Nat. Phys.* **9**, 795–800 (2013).
8. G. Jotzu *et al.*, *Nature* **515**, 237–240 (2014).
9. M. Aidelsburger *et al.*, *Nat. Phys.* **11**, 162–166 (2015).
10. L. M. Nash *et al.*, *Proc. Natl. Acad. Sci. U.S.A.* **112**, 14495–14500 (2015).
11. R. Süsstrunk, S. D. Huber, *Science* **349**, 47–50 (2015).
12. J. Ningyuan, C. Owens, A. Sommer, D. Schuster, J. Simon, *Phys. Rev. X* **5**, 021031 (2015).
13. T. Karzig, C.-E. Bardyn, N. H. Lindner, G. Refael, *Phys. Rev. X* **5**, 031001 (2015).
14. A. V. Nalitov, D. D. Solnyshkov, G. Malpuech, *Phys. Rev. Lett.* **114**, 116401 (2015).
15. L. Lu, J. D. Joannopoulos, M. Soljačić, *Nat. Photonics* **8**, 821–829 (2014).
16. T. Ozawa *et al.*, *Rev. Mod. Phys.* **91**, 015006 (2019).
17. A. Barthelemy, S. Maneuf, C. Froehly, *Opt. Commun.* **55**, 201–206 (1985).
18. D. N. Christodoulides, R. I. Joseph, *Opt. Lett.* **13**, 794–796 (1988).
19. M. Segev, B. Crosignani, A. Yariv, B. Fischer, *Phys. Rev. Lett.* **68**, 923–926 (1992).
20. H. S. Eisenberg, Y. Silberberg, R. Morandotti, A. R. Boyd, J. S. Aitchison, *Phys. Rev. Lett.* **81**, 3383–3386 (1998).
21. G. I. Stegeman, M. Segev, *Science* **286**, 1518–1523 (1999).
22. J. W. Fleischer, M. Segev, N. K. Efremidis, D. N. Christodoulides, *Nature* **422**, 147–150 (2003).
23. M. S. Rudner, N. H. Lindner, E. Berg, M. Levin, *Phys. Rev. X* **3**, 031005 (2013).
24. S. Mukherjee *et al.*, *Nat. Commun.* **8**, 13918 (2017).
25. L. J. Maczewsky, J. M. Zeuner, S. Nolte, A. Szameit, *Nat. Commun.* **8**, 13756 (2017).
26. Y. Lumer, Y. Plotnik, M. C. Rechtsman, M. Segev, *Phys. Rev. Lett.* **111**, 243905 (2013).
27. M. J. Ablowitz, C. W. Curtis, Y.-P. Ma, *Phys. Rev. A* **90**, 023813 (2014).
28. D. Leykam, Y. D. Chong, *Phys. Rev. Lett.* **117**, 143901 (2016).
29. J. L. Marzuola, M. Rechtsman, B. Osting, M. Bandres, arXiv 1904.10312 [cond-mat.mes-hall] (21 April 2019).
30. M. Büttiker, *Phys. Rev. B* **38**, 9375–9389 (1988).
31. See supplementary materials.
32. S. Mukherjee, H. K. Chandrasekharan, P. Öhberg, N. Goldman, R. R. Thomson, *Nat. Commun.* **9**, 4209 (2018).
33. T. Kitagawa, E. Berg, M. Rudner, E. Demler, *Phys. Rev. B* **82**, 235114 (2010).
34. A. Szameit *et al.*, *Opt. Express* **14**, 6055–6062 (2006).
35. Y. Cao *et al.*, *Nature* **556**, 43–50 (2018).
36. L. W. Clark, N. Schine, C. Baum, N. Jia, J. Simon, arXiv 1907.05872 [cond-mat.quant-gas] (12 July 2019).
37. Y. Hadad, A. B. Khanikaev, A. Alu, *Phys. Rev. B* **93**, 155112 (2016).
38. D. Leykam, S. Mittal, M. Hafezi, Y. D. Chong, *Phys. Rev. Lett.* **121**, 023901 (2018).
39. L. He *et al.*, *Nat. Commun.* **10**, 4194 (2019).
40. S. Kruk *et al.*, *Nat. Nanotechnol.* **14**, 126–130 (2019).
41. D. Smirnova *et al.*, *Phys. Rev. Lett.* **123**, 103901 (2019).

ACKNOWLEDGMENTS

We thank H. K. Chandrasekharan, J. Guglielmon, D. Leykam, and J. Noh for useful discussions and N. C. Giebink for use of a supercontinuum laser source for directional coupler characterization. **Funding:** Supported by Office of Naval Research award N00014-18-1-2595 (S.M. and M.C.R.) and by Packard Foundation fellowship 2017-66821 and Kaufman Foundation award KA2017-91788 (M.C.R.). **Author contributions:** S.M. designed and built the waveguide fabrication system as well as characterization setups and carried out all experiments; S.M. and M.C.R. conceived the idea, designed the experiment, analyzed data, and wrote the manuscript; S.M. performed theoretical analysis with input from M.C.R.; M.C.R. supervised the project. **Competing interests:** The authors declare no competing interests. **Data and materials availability:** All associated data and materials are available in the manuscript and supplementary materials.

SUPPLEMENTARY MATERIALS

science.sciencemag.org/content/368/6493/856/suppl/DC1
Supplementary Text
Figs. S1 to S9
Movies S1 to S5
References (*42*–*46*)

12 January 2020; accepted 14 April 2020
10.1126/science.aba8725

Observation of Floquet solitons in a topological bandgap

Sebabrata Mukherjee and Mikael C. Rechtsman

Science **368** (6493), 856-859.
DOI: 10.1126/science.aba8725

Topological insulators go nonlinear

Whereas solid-state insulators tend to be fixed by material properties, photonic topological insulators can be designed at will to mimic a variety of scenarios and complex interactions. Mukherjee and Rechtsman go beyond the linear optical regime that has been studied to date and show that photonic topological insulators can also exhibit nonlinear optical features (see the Perspective by Ablowitz and Cole). Their array of laser-written waveguides can support solitons, which are also found to exhibit topological features, performing cyclotron-like orbits associated with the topology of the lattice. The nonlinear properties provide a rich playground for further exploration, with the possibility of mimicking other interacting bosonic systems.

Science, this issue p. 856; see also p. 821

Science (print ISSN 0036-8075; online ISSN 1095-9203) is published by the American Association for the Advancement of Science, 1200 New York Avenue NW, Washington, DC 20005. The title *Science* is a registered trademark of AAAS.